Appendix M: Assessment of Finite Length Defects

1 Overview

In TWI Report 24000-9-15, the critical defect depth of fully-circumferential surface flaws under topple test was calculated. This was determined to be 1.1mm when some allowance for stable ductile tearing is taken into consideration for the average joint geometry (TWI, 2015).

However, in the post-mortem and metallographic examination phase of the research programme, two surface flaws, each approximately 50mm long, were identified in sections of circumferential weld removed from GRW tanker J3564. Both flaws had depths in excess of 2.0mm, but it was not possible to conclusively state whether such defects would lead to likely failure under topple test conditions. Therefore, additional numerical and analytical work was required to determine the criticality of such finite length surface flaws.

2 Objective

- To determine the critical defect depth for a circumferentially-oriented, 50mm long, internal surface flaw in a GRW joint under topple test conditions.

3 Approach

3.1 Software

All finite element models were generated using version 6.14-1 of the pre-processing finite element software Abaqus/CAE and the analyses were solved using version 6.14-1 of Abaqus/Standard (SIMULIA, 2014).

3.2 Geometry

In order to model the finite length surface flaws, three-dimensional models of a local section of the GRW circumferential extrusion band joint were generated.

The solid geometry was created by revolving the (uncracked) axisymmetric cross-section of the average joint geometry 45^{o} around the axis of the tank (so that 1/8th of the dish and extrusion band joint geometry was modelled). For consistency with the earlier fully-circumferential flaw study, the model assumes a circular cross section of the tanker with mean radius 2000mm; weld cap height 1.97mm; weld cap width 15.6mm, and misalignment equal to 0.63mm. A small axial length of the 5mm thick tanker shell either side of the extrusion band was included in the model and used to apply the loads and boundary conditions. No additional internal fillet or tack weld was included in the geometry. The decision to exclude this feature from the geometry was based on previous analyses which showed that, when the additional internal fillet weld is present (and of suitable size), the failure of the circumferential joint does not occur in the section containing the defect, but in the tanker shell. Additional details about the local geometry of the axisymmetric cross-section of the average joint geometry can be found in the main report.

A cylindrical coordinate system (r,θ,z) was employed with the usual orientation: r corresponding to the radial coordinate, θ the angular coordinate, and the z-axis aligned with the axis of the extrusion band and dish. For convenience, the crack was located at the 'top' of the model, ie at θ = π/2. A symmetry plane perpendicular to the crack plane and passing through the mid-point of the crack (ie the θ=π/2 plane) was assumed; hence the 1/8th geometry modelled ¼ of the total dish-to-extrusion band section.

The geometry was divided into two distinct parts: a crack block and global part. The global part contained the dish, extrusion band and tanker shell and subtended most of the modelled circumference but had a small, local block containing the cracked section removed. The 'crack block' was located at the top of the model and contained the finite length crack. The different parts of the model are illustrated in Figure M1. As described in Appendix K, the finite length defects that were observed in the sections from J3564 were typically offset from the positioner lip by about 1.0-2.0mm, had maximum depth in excess of 2.0mm and total surface length approximately 50mm. A macro from J3564 is shown in Figure M2 to illustrate the typical cross-section of the defect. Further details are provided in Appendix K. Therefore, in the crack block, the crack plane was positioned 2.0mm offset in the axial direction from the positioner lip. The crack front geometry assumed a canoe-shaped crack front. Cracks were modelled with depths ranging from 1.50mm to 3.00mm. All cracks had constant crack length, 2c = 50mm. Due to symmetry, only half of the crack was modelled.

The entire model was meshed with 20-node, quadratic, hexahedral elements with reduced integration (type C3D20R in Abaqus). The crack front was meshed with the standard swept crack tip rosette mesh. The inner-most tube of elements surrounding the crack front comprised collapsed wedge elements with duplicate node degeneracy to allow for crack tip blunting. The crack tip elements were then surrounded by seven concentric rings of elements with each element subtending an angle of approximately 15^{o}. The crack block was meshed more densely than the global part, but all parts had several elements (typically more than 6) through thickness in order to accurately resolve the nonlinear, elastic-plastic through-wall bending stress profile. Images of the finite element mesh are shown in Figure M3. The incompatible element faces on the interface surfaces between the crack block and the global part were joined by a tie constraint as described in Section 3.4.

3.3 Material properties

As detailed in Section 4.4.2 of the main report, tensile testing was undertaken on metal samples from GRW tankers J3025 and J3146. Details of the tensile testing are provided in Appendix H. The stress-strain curves for the parent metal samples showed only small variation between the two different tankers. The weld metal stress-strain curves showed larger differences, but the overall level of partial under- or partial over-matching was small. All of the tensile stress-strain curves are shown in Figure M4.

A weld metal sample from J3025 (labelled ROUND TENSILE 23437 W01-07 in Figure M4) produced a lower bound stress-strain curve. This curve was sampled at equally spaced points and converted from engineering stress and engineering strain to true stress and true plastic strain. A rate-independent plasticity model using the von Mises yield criterion and isotropic strain hardening rule was implemented in the model based on the sampled points shown in Figure M4. The linear elastic constants for the model were 70,000MPa for the Young's modulus and 0.3 for Poisson's ratio.

3.4 Loads and boundary conditions

As part of the Department for Transport research on petroleum tankers, the Health and Safety laboratory (HSL) undertook detailed fluid-structure interaction modelling of the topple testing of non-compliant GRW tankers. For the simulation involving the tanker filled with fuel oil and an initial rotational velocity of 2.6rad/s, HSL predicted that a section approximately 250mm long of the circumferential weld is acted on by a normalised bending moment of

1460N.mm/mm. This normalised bending moment defines the so-called 'topple test' load case. Assuming a Ramberg-Osgood representation of the stress-strain curve and a rectangular cross-section with length 1.0mm (unit length in the circumferential direction) and height 5.0mm (the tanker shell wall thickness), the through-wall, elastic-plastic bending stress generated by this bending moment is 254MPa. Taking into consideration that the HSL simulation employed the actual, non-circular cross-sectional geometry of the GRW tanker and that the previous TWI axisymmetric model assumed a circular cross-section with mean radius 2000mm, the bending moment had to be modified in order to generate the same through-wall, elastic-plastic bending stress. The modified, normalised moment for the circular cross-section was approximately 1630N.mm/mm. This was verified with preliminary, uncracked stress analyses.

The bending moment generates a through-wall bending stress in the tanker shell wall. In a three-dimensional model, this means that the bending moment acts about the circumferential coordinate with the neutral plane aligned with the mid-plane of the tanker shell. In order to apply the bending moment to the $1/8^{th}$ model containing the finite length defects, reference nodes were created at nearly equally spaced intervals around the circumference of the leading end (ie positive z-direction) of the tanker shell. The spacing was typically 100mm between reference nodes and the reference nodes were positioned radially so that they were located along the mid-plane of the tanker shell. The 3D tanker shell geometry was then partitioned into sections of 100mm circumferential length corresponding to the reference node positioning. The axial degree of freedom of each section of tanker shell face on the (r,θ)-plane was kinematically coupled to the corresponding reference node. The total normalised moment of 1630N.mm/mm was distributed amongst the reference nodes with the actual moment applied at each reference node being based on the proportion of cross-sectional area coupled to the reference node. This is illustrated in Figure M5. Each of the reference nodes was restrained in all other degrees of freedom except for the axial degree of freedom and the rotational degree of freedom about the circumferential coordinate. The trailing end of the tanker shell (ie negative z-direction side) was restrained in the axial direction, and to model the circumferential symmetry planes for the $1/8^{th}$ sector model, the circumferential displacement degree of freedom was restrained on the $\theta=\pi/2$ and $\theta=\pi/4$ planes. These boundary conditions are illustrated in Figure M6. All models were analysed with small strain (linear geometry) assumptions.

4 Results

The typical deformation mode of the local section containing the crack is shown in Figure M7 for a 2.5mm deep crack. In this figure, the top frame shows the von Mises stress contour and the bottom frame shows the equivalent plastic strain (PEEQ) contour. As discussed in the main report, the topple test load case results in extensive through wall yielding of the tanker shell, as evidenced by the positive PEEQ (non-blue) regions in the bottom frame of Figure M7.

For each simulation, the J-integral was calculated from up to 10 contours surrounding the crack tip. Path-independence of the J-integral was verified for each simulation and the value of J reported was obtained from the outermost contour. A plot of crack driving force (J_{app} or applied J-integral) as a function of crack depth was generated and is shown as the black line with square symbols in Figure M8.

In addition to tensile testing, fracture toughness testing was undertaken on sub-size SENB specimens machined from weld metal samples from GRW tankers. The details of the fracture toughness testing are provided in

Appendix H. The result of the fracture toughness testing was a tearing-resistance or R-curve that represents the increase in effective fracture toughness as a crack grows by stable ductile tearing. The combined R-curve described in Section 4.4.3 of the main report is represented by the equation:

$$J_{mat} = 9.35 + 63.8(\Delta a)^{1.00}$$

Where J_{mat} is the effective material fracture toughness and Δa is the amount of crack extension. Starting from an initial defect depth a_0 this curve represents the material toughness as a function of crack extension. This is shown as the solid red line in Figure M8.

The tearing instability point is defined as the point at which the material toughness and applied crack driving force curves are tangent. To determine this tangency point, a fourth order polynomial was fitted to the crack driving force versus crack depth curve. The polynomial was then differentiated to determine the point at which the crack driving force curve and tearing-resistance curve were tangent (ie had the same slope). This is shown as the green dot in Figure M8. Tracing the R-curve back from the tearing instability point allows determination of the critical defect depth as described in more detail in the main report. For the 50mm long surface defects, the critical defect depth was determined to be 1.35mm.

5 Conclusions

A series of *a* x 50mm surface flaws have been modelled in the GRW extrusion band joint with average joint geometry and without additional internal fillet weld, where a is the crack depth and ranged from 1.5mm to 3.0mm. For each modelled flaw, the J-integral arising from the topple test load case was calculated. By generating a curve of crack driving force versus crack depth and comparing it with the corresponding tearing-resistance curve, the maximum acceptable defect depth for a 50mm long surface crack was determined to be 1.35mm. Therefore, defects with dimension a x 50mm with a > 1.35mm in a GRW circumferential weld with average geometry and no additional internal fillet weld would lead to likely rupture of the circumferential weld under topple test conditions.

This critical defect depth for 50mm long flaws is less than the maximum defect depth observed in the sections from J3564. However, the 50mm long surface defects found in the sections from J3564 had additional internal fillet welds present and would therefore not likely lead to rupture of the weld.

6 References

TWI (2015): 'Department for Transport Technical Assessment of Petroleum Tankers: Work Package 2 – Detailed Engineering Critical Assessment', TWI Report 24000/9/15.

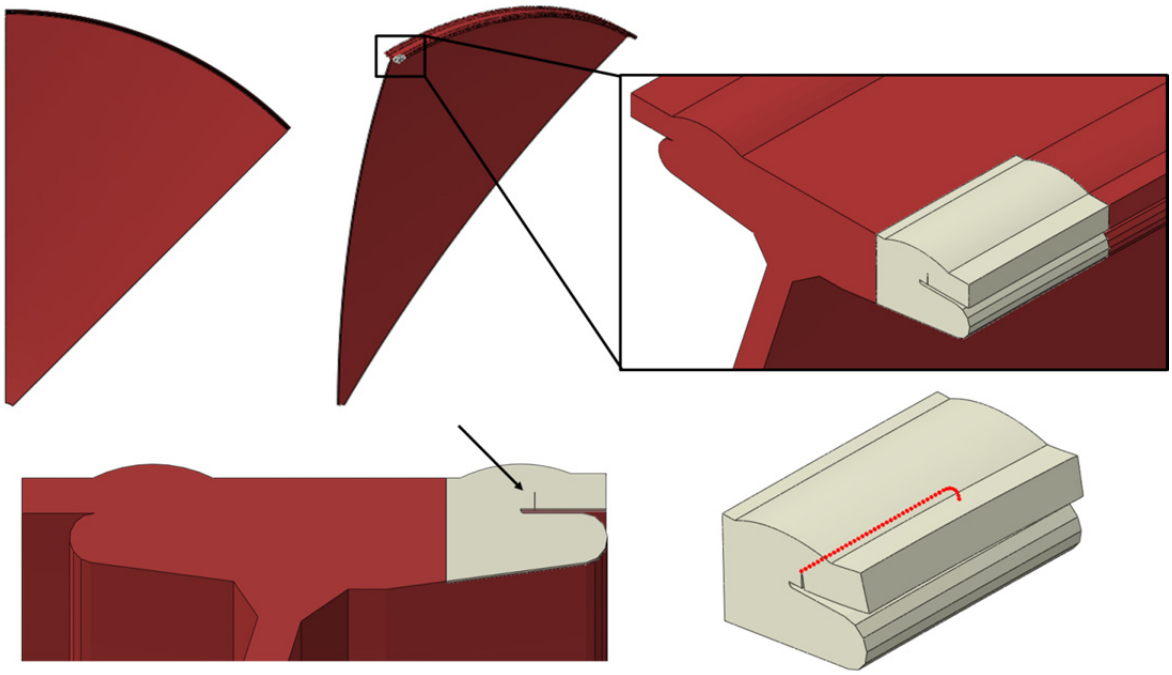

Figure M1 Diagrams of the three-dimensional geometry. The red regions represent the global part and the beige region is the crack block. The arrow highlights the offset crack plane from the location considered for the fully-circumferential flaws. The red curve in the bottom right frame is half of the crack front.

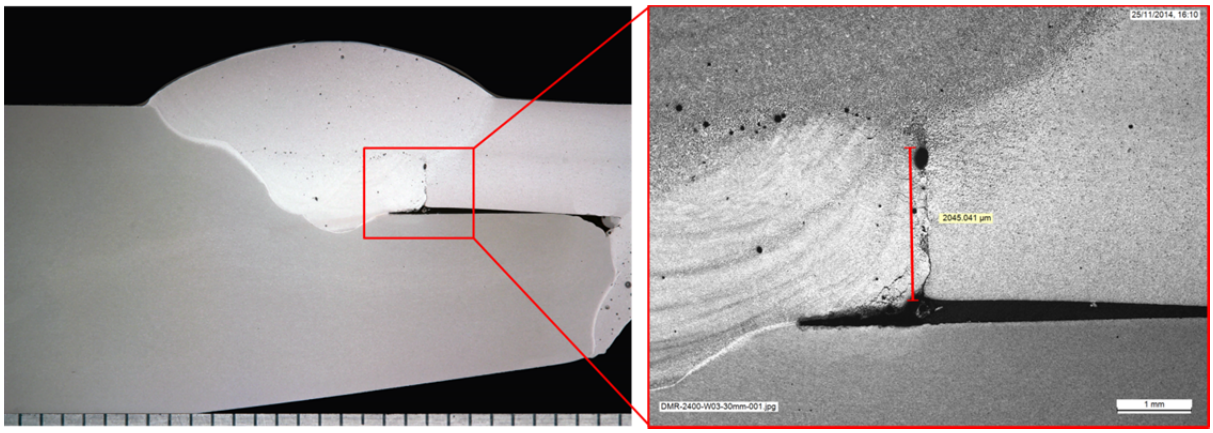

Figure M2 Section from J3564 showing part of the 50mm long surface defect. In the right frame, the scale bar is 1.0mm and the crack has depth 2.045mm. In the left frame, the scale bars indicate 1.0mm.

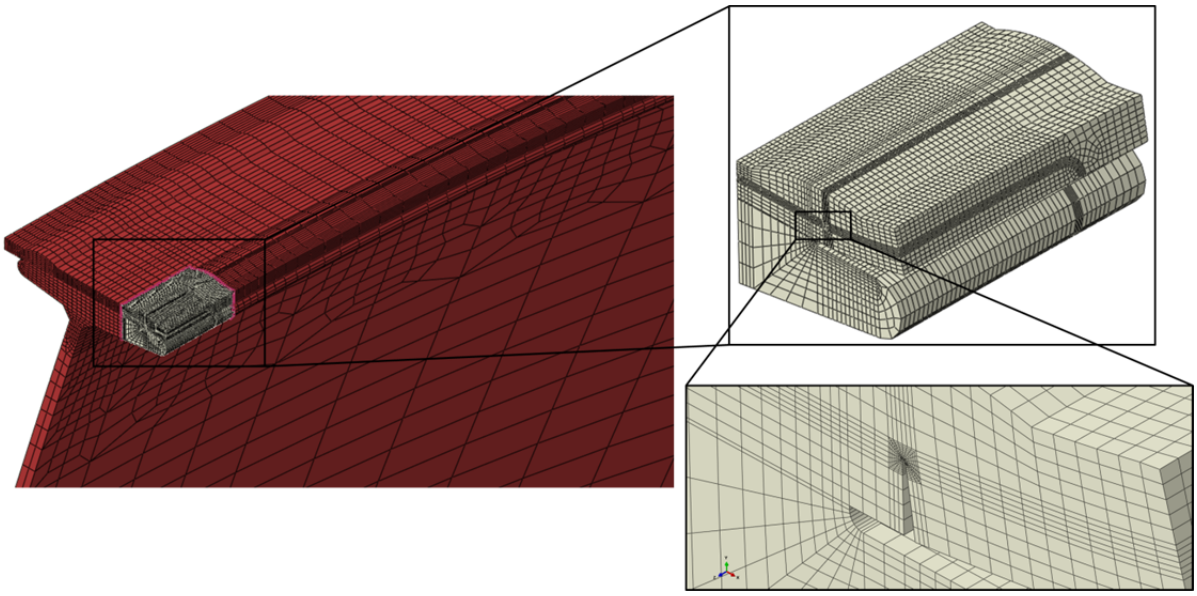

Figure M3 Illustration of the typical finite element mesh. Crack shown is 2.5mm deep.

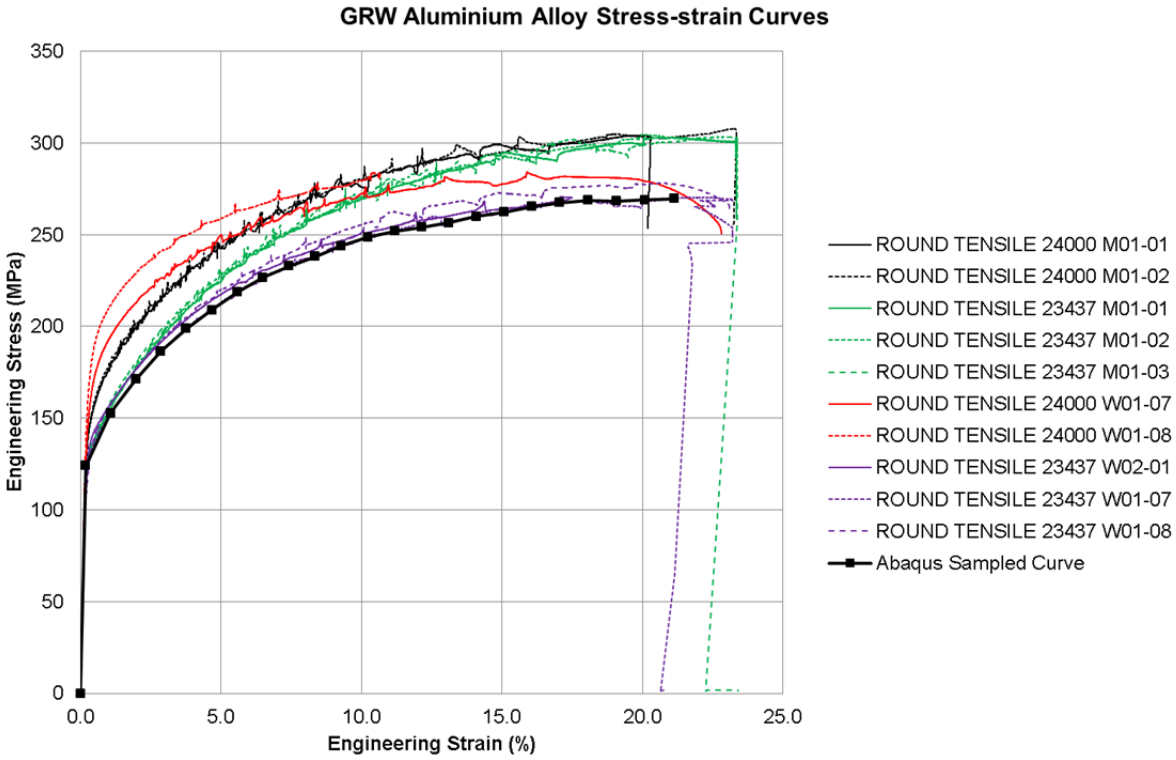

Figure M4 Tensile stress-strain curves for parent and weld metal. Black dark line shows the sampled data points used for the finite element models.

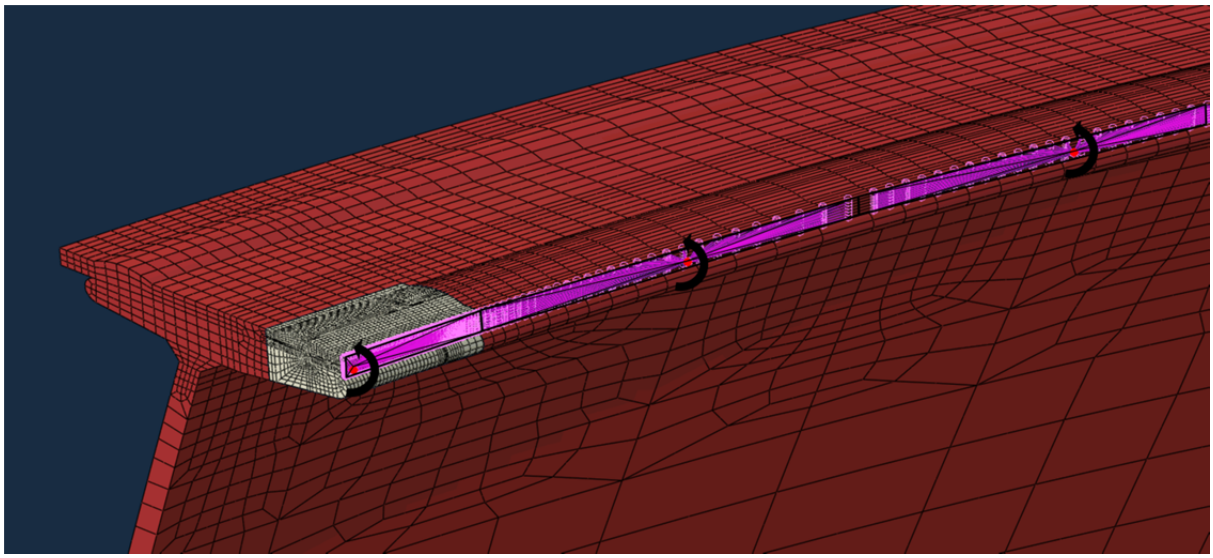

Figure M5 Illustration of the load coupling of the leading end of the tanker shell for application of the bending moment about the circumferential coordinate.

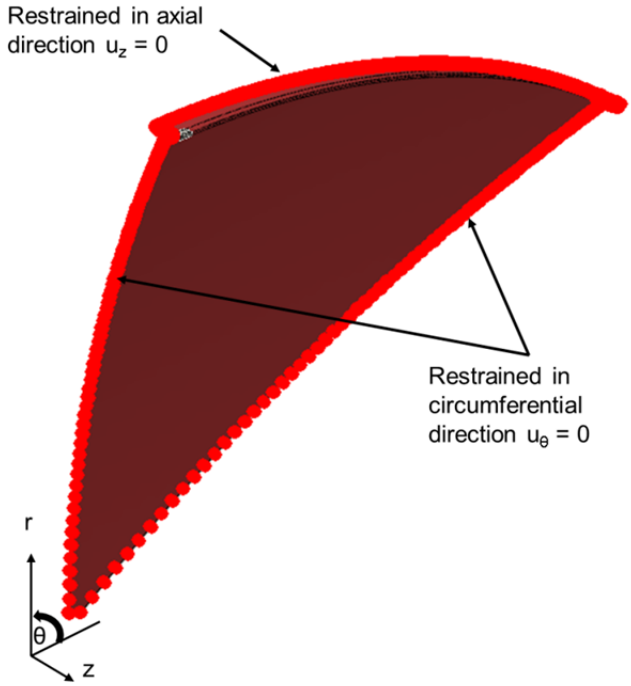

Figure M6 Illustration of the boundary conditions in the cylindrical coordinate system.

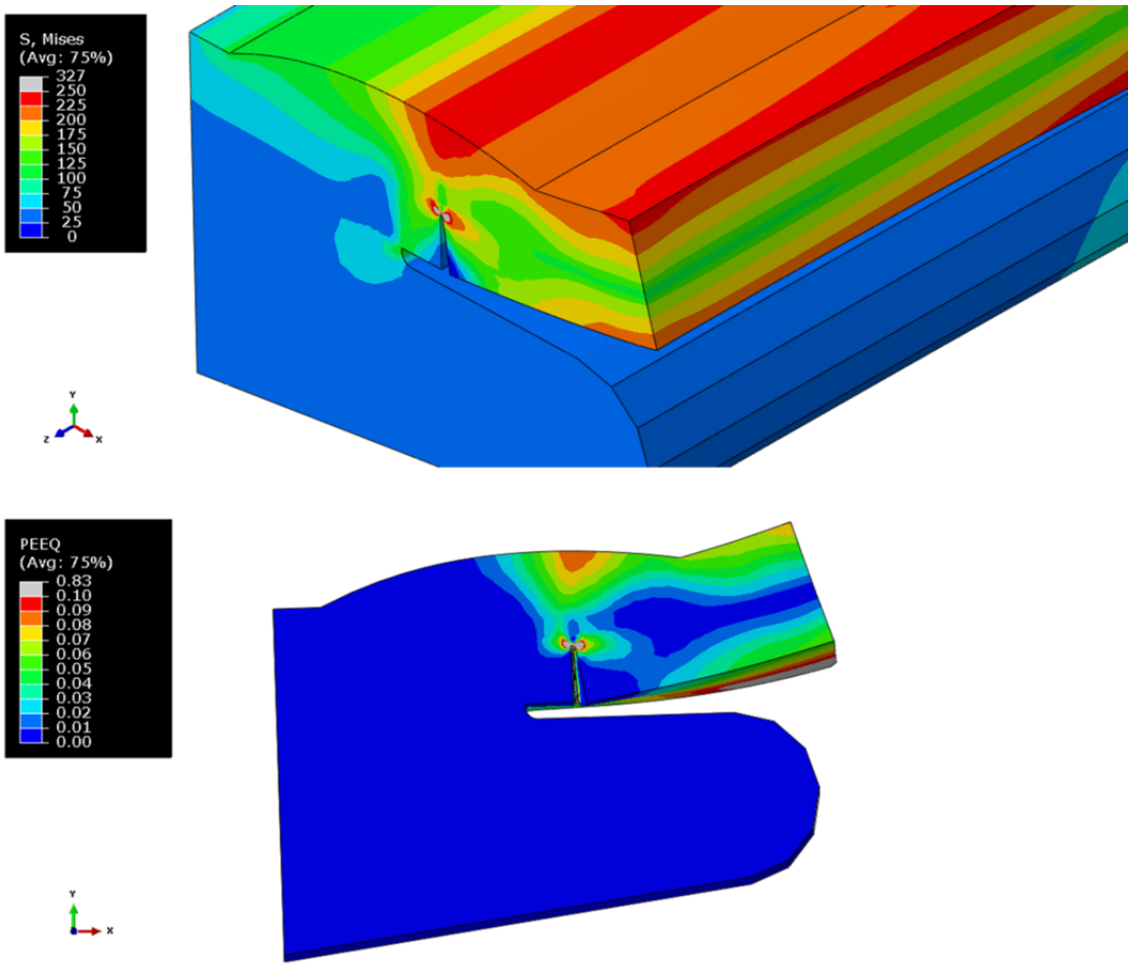

Figure M7 Von Mises stress contour (top frame) and equivalent plastic strain contour (bottom frame) for a model of a 2.5mm by 50mm long surface crack.

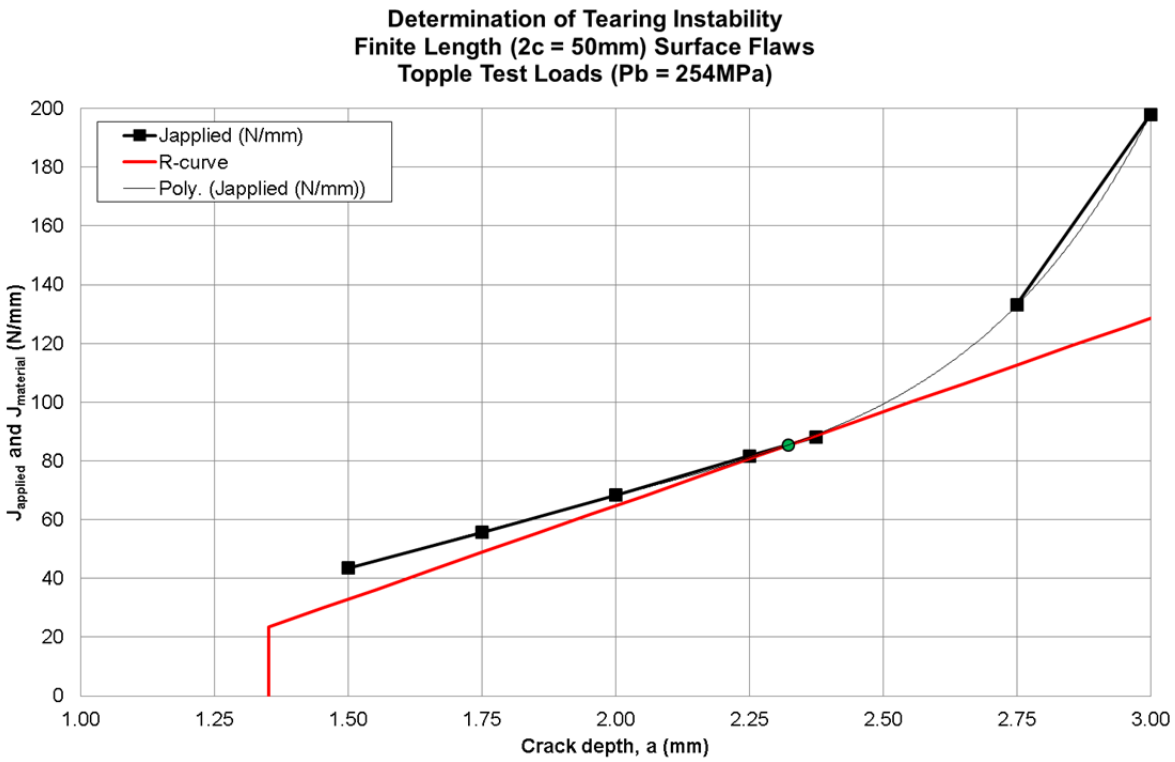

Figure M8 Plot of crack driving force (J-applied) and tearing resistance (R-curve) as a function of crack depth. The polynomial interpolant was used to identify the tearing instability, tangency point.